Synergetic p+n Field-Effect Transistor Circuits for ppb-Level Xylene Detection

Xinyuan Zhou, Ying Wang, Zhou Wang, Liping Yang, Xiaofeng Wu, Ning Han, and Yunfa Chen

***Abstract*— Nowadays, xylene is not only one major air pollutant which threats human health even if its concentration is lower than the human olfactory threshold of 470 ppb, but also one of the typical gases exhaled by the lung cancer patients with a criterion of 10-20 ppb. However, *in situ* detection of the ppb-level xylene for air quality monitoring and breath analysis remains challenging using the easily fabricated and low cost metal oxide semiconductor gas sensors. Herein, a synergetic p + n field effect transistor (FET) amplification circuit is designed to detect the ppb level xylene. By optimizing the load resistor (R_L) and the p- and n-FET coupling effect, a magnification factor (∼7.5) is obtained. This amplification circuit decreases the detection limit of TGS2602 sensor to ∼10 ppb xylene with apparent response of about 2.3 and voltage change of >0.5 V, promising for air quality monitoring (the highest permissive limit of 42 ppb) and breath disease analysis (threshold of lung cancer 10–20 ppb). The mechanism is that the matched couple of p + n FETs work synchronically when their ($R_L + R_{FET}$) − I curves nearly coincide with each other. All those results show the prospect of ppb level gas detection with MOX sensors using the synergetic p + n FET amplification circuit.**

***Index Terms*— Environment and health, field effect transistor, trace concentration xylene, amplification effect, metal oxide semiconductor sensor.**

I. Introduction

XYLENE is one of the most important industrial solvents used for paints, adhesive materials, etc. As a result, it is one of the most representative and ubiquitous indoor toxic gases that are emitted from the indoor decorations and will induce various symptoms, including irritation of the skin, eyes, and respiratory system even at low concentrations [1], [2]. The highest permissive detection limit is therefore strictly limited all over the world, such as the limit of 0.2 mg/m^3 (∼42 ppb) in China (GB/T 18883-2002). In the meanwhile, xylene is also one of the typical biomarkers (benzene derivatives) related to lung cancer with a criterion of 10-20 ppb [3], as examined by many measurements such as colorimetric device by Zhao *et al.* [4] gas chromatography by Oguma *et al.* [5] and Ma *et al.* [6]. Therefore, fast and effectively detecting xylene in ppb level is important and necessary as to monitoring the indoor air quality and also to fast screening the disease [7]–[10]. Although precise and reliable xylene detection can be realized by gas chromatograph spectroscopy [11]–[13] and fluorescence spectroscopy [14] etc., there are some major hurdles for real-time monitoring in sampling, high cost, and prolonged analysis time. Therefore, more and more attention has been paid to the metal oxide semiconductor (MOX) gas sensors due to their advantages of low cost, facile method, easy fabrication and real time monitoring [15]–[21]. However, though MOX sensors are successful in ppm level gas detection such as ethanol [22], [23], acetone [24]–[26], CO [27], [28] etc., it is still challenging for MOX sensors to detect xylene at ppb level, due to the relatively low response at this trace concentration.

To enhance the gas response of MOX sensors, developing highly sensitive MOX materials is widely investigated. And many oxide semiconductors have been synthesized by designing the hierarchical structure and heterostructures, including α-MoO_3/α-Fe_2O_3 heterostructures [29], Pd-loaded SnO_2 yolk–shell spheres [30], Pd-loaded Co_3O_4 hollow nanostructures [31], Ni-doped TiO_2 bowllike submicron particles [32], Co-doped branched ZnO nanowires [33], Cr-doped NiO hierarchical nanostructures [34] and double-layered metal-oxide thin film [35] . Though these researches make the xylene MOX sensors more sensitive at ppm level, there is still few MOX sensors reported in the literature capable to detect the xylene at ppb level, nor can most of commercial sensors. And recently, pre-concentrator is developed to detect benzene with response of 1.2 to 100 ppb [36].

From the electronics viewpoint, electronic interfaces are widely investigated and the voltage signal of MOX sensors can be amplified by operational amplifier [37]–[40] . However, the integrated circuits should be complicatedly designed as most MOX sensors are working at a low voltage baseline and then giving a signal of high voltage, and special care should be taken to the noise filtering. All these are considered by the application engineers and the complex circuit design and integration would degenerate the advantage of easy-fabrication and low-cost of MOX sensors. And Wang et al. have developed p+n combined gas sensor array to enhance the response of single p or n type gas sensor [41] , which however is not

Manuscript received February 11, 2018; accepted March 20, 2018. Date of publication March 23, 2018; date of current version April 9, 2018. This work was supported in part by the National Key Research and Development Program of China under Grant 2016YFC0207100, in part by the National Natural Science Foundation of China under Grant 51272253, in part by the Guangdong Innovative and Entrepreneurial Research Team Program under Grant 2014ZT05C146, and in part by the State Key Laboratory of Multiphase Complex Systems under Grant MPCS-2014-C-01. The associate editor coordinating the review of this paper and approving it for publication was Dr. Chirasree Roychaudhuri. *(Corresponding author: Ning Han.)*

The authors are with the State Key Laboratory of Multiphase Complex Systems, Institute of Process Engineering, Chinese Academy of Sciences, Beijing 100190, China, and with the University of Chinese Academy of Sciences, Beijing 10049, China, and also with the Center for Excellence in Regional Atmospheric Environment, Institute of Urban Environment, Chinese Academy of Sciences, Xiamen 361021, China (e-mail: zhouxinyuan14@mails.ucas.ac.cn; nhan@ipe.ac.cn; chenyf@ipe.ac.cn).

This paper has supplementary downloadable multimedia material available at http://ieeexplore.ieee.org provided by the authors. The Supplementary Material contains measured IV curves of FETs, and sensor responses of Figures S1-S14. And the response/recovery times of Table S1. This material is 671 KB in size.

Digital Object Identifier 10.1109/JSEN.2018.2818710

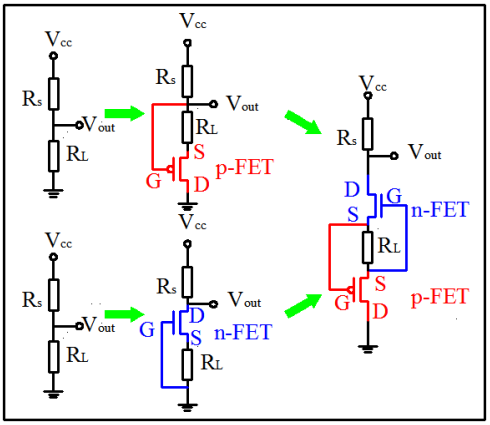

Fig. 1. Design scheme of the conventional electric circuit, designed single p- and n-FET amplification circuit and synergetic p+n amplification circuit for MOX xylene sensors.

widely applied till now due to the lack of highly sensitive p-type MOX sensors.

In our previous study, we reported an easy n-type field effect transistor (n-FET) amplification circuit to amplify the voltage signal of MOX sensors. In this study, p-FET analogue amplification circuit is developed. However, differing from traditional complementary metal oxide semiconductor (CMOS) design, the p+n FETs are further synergistically integrated into an amplification circuit to increase the voltage signal of MOX sensors taking commercial sensor (Figaro TGS2602, Japan) as an example. Using this sensor circuit, absolute voltage output of 1.0 V is obtained for 20 ppb xylene, corresponding to an apparent response of 5.4. Further detection limit of < 10 ppb (response about 2.3) is derived by the regression calculation, which is one of the highest in the literature. And more importantly, all these electronic elements can be purchased from the market, implying the good reproducibility and long-term stability.

II. Design Scheme of the Amplification Circuit

To make a comparison and to interpret the synergetic amplification effect, the tradition and our proposed circuits are schematically drawn in Figure 1. Considering n-type MOX sensor (R_S) detecting xylene, it is connected in tandem to a load resistor (R_L) in the traditional circuit. A bias voltage (V_{cc}) is used for the test, and the partial voltage of the R_L is the sensor signal (V_{OUT}). Generally, V_{OUT} in clean air is low behaving as the baseline, which will then increase to generate the signal because R_S will decrease when the sensor gets in contact with xylene. Therefore, it is merely the decrease of R_S that generates the signal.

The p-FET (depletion mode) amplification circuit is proposed in Figure 1 to connect with R_L at the source (S) electrodes and the drain (D) is connected to ground. The gate electrode (G) is then connected to the higher potential side of R_L generating a positive gate voltage for the p-type FET. The value of R_L is well chosen so as to make the p-type FET work at ON state in clean air. Similar to the traditional circuit, V_{OUT} will also increase when the sensor contacts xylene. This would also induce an increase of the gate to source voltage (V_{GS}) of the p-type FET, which will turn off the p-type FET, i.e. the resistance of the p-FET will increase dramatically. The increased p-FET resistance gives feedback to the circuit again to enhance the V_{OUT}, higher than that without the p-FET. Using this principle, n-FET amplification circuit is also designed as reported in previous study [42].

Then, the p-FET and n-FET are synergistically combined to design the amplification circuit as shown in Figure 1 in an aim to enhance the amplification factor. Similarly, both p- and n-FETs are at ON state using appropriate R_L. And in contact with xylene, both $|V_{GS}|$ of the two FETs will increase to turn OFF them. Obviously, both of p-type and n-type FETs amplify the V_{OUT} synchronically, which causes larger V_{OUT} than those of single p- and n-FET amplification circuit, not to say the traditional non-amplified circuits.

III. Experimental

Xylene gas sensors (Figaro TGS2602, Japan) are bought from the market, and so do the commercial FETs, which are 2SK163 (Hitachi, Japan), 2SK544 (Sanyo, Japan), 2SK30ATM (Toshiba, Japan), 2SJ45 (NEC, Japan), 2SJ44 (NEC, Japan), and 2SJ164 (Panasonic, Japan). All the electronic devices above are used without any modification. The I_{DS} - V_{DS} and I_{DS} - V_{GS} curves of the FETs are measured by Keithley 4200 semiconductor analyzer. The gas sensing property is measured using static measurement system designed for sensor products (Hanwei WS-30A, China) as details reported in the literature [43]–[46]. Load resistance card is the standard accessory of the system, and the FET is soldered onto the resistance card with D, S, and G electrodes shown in Figure 1. Different xylene concentrations ($\geq$0.5 ppm) are generated by dropping certain amounts of the liquid xylene with a micro syringe onto an evaporator in the test chamber (total volume 18 L). Xylene gases with 0.02, 0.04, 0.1 and 0.2 ppm are produced by adding certain volume of 20 ppm standard gas into the chamber. R_{Sa} and R_{Sg} are sensor resistances (R_S) in air and in xylene gas, which are calculated as:

$$R_{Sa} = R_L(V_{CC} - V_{OUT,a})/V_{OUT,a}. \quad (1)$$

$$R_{Sg} = R_L(V_{CC} - V_{OUT,g})/V_{OUT,g}. \quad (2)$$

where V_{CC} is 5 V, R_L is the load resistance and V_{OUT} is the measured voltage response. Then response in traditional circuit is defined as:

$$R_{Sa}/R_{Sg} = (V_{CC}/V_{OUT,a} - 1)/(V_{CC}/V_{OUT,g} - 1) \quad (3)$$

As to FET amplification circuit, R_{Sa} and R_{Sg} are calculated in same way:

$$R_{Sa} = (R_L + R_{FET,a})(V_{CC} - V_{OUT,a})/V_{OUT,a}. \quad (4)$$

$$R_{Sg} = (R_L + R_{FET,g})(V_{CC} - V_{OUT,g})/V_{OUT,g}. \quad (5)$$

Thus the magnification factor (MF) is $(R_L + R_{FET,g})/(R_L + R_{FET,a})$. i.e. resistance change of the load $(R_L + R_{FET})$.

IV. Results and Discussion

A. p-FET Amplification Circuit

Figaro TGS2602 MOX sensor is developed for toluene, with no response data to xylene in the manual. To estimate the

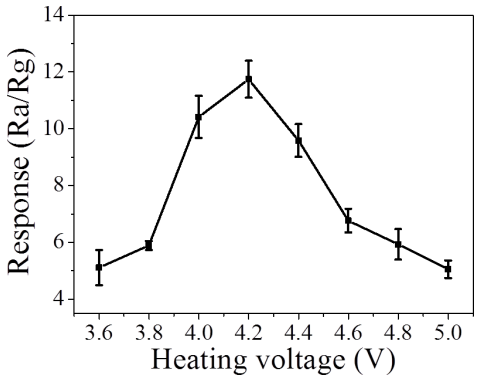

Fig. 2. Response curve of TGS2602 to 1 ppm xylene gas in the traditional circuit without FET (statistics of 20 sensors) when the gas sensor is heated by heating voltages from 3.6 to 5.0 V with a step of 0.2 V.

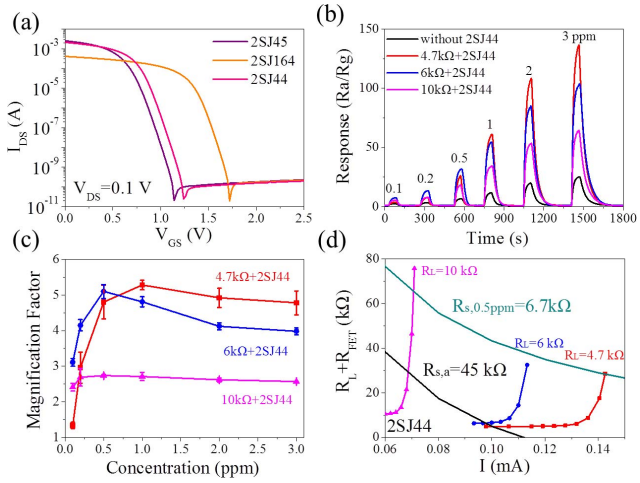

Fig. 3. Amplification effect of p-FET amplification circuits: (a) I_{DS}-V_{GS} curves of FETs 2SJ44, 2SJ45 and 2SJ164, (b) response of TGS2602 to xylene from 0.1 to 3 ppm in the electric circuit with and without FET 2SJ44, (c) magnification factors of the amplification circuit with FET 2SJ44, and (d) the curves of $(R_L + R_{FET}) - I$ by connecting resistors of R_L = 4.7, 6.0 and 10.0 kΩ. The intersection points with $5/I - R_{S,a}$ and $5/I - R_{S,0.5ppm}$ curves are the $(R_L + R_{FET})$ value in air and in 0.5 ppm xylene.

xylene sensing property, 1 ppm xylene gas is tested in the traditional circuit without FET when gas sensor is heated by different voltages from 3.6 to 5.0 V as shown in Figure 2. It is clear that the response has a peak value of 11.74 ± 0.65 (20 sensors) when the heating voltage is 4.2 V. Therefore, 4.2 V is the optimum heating voltage adopted in the following experiments.

The transfer curves (I_{DS} - V_{GS}) of typical p-FETs are measured as shown in Figure 3a, where both 2SJ44 and 2SJ45 FETs have larger I_{DS}-V_{GS} slopes (the smallest sub-threshold swings) compared with 2SJ164 FET. The larger slope makes FET more sensitive to the gate voltage change, leading to the larger amplification effect according to our previous work [42]. From the working principle in Figure 1, the V_{GS} of FET is the partial voltage of the resistor load R_L, which should therefore be optimized to get a maximum amplification. In our study, R_L is set as 4.7, 6.0 and 10.0 kΩ, and the typical response curves with and without FET 2SJ44 are shown in Figure 3b). It is clear that responses to xylene from

TABLE I

THEORETICAL AND ACTUAL MAGNIFICATION FACTORS (MF) OF FETS 2SJ44, 2SK544, 2SJ44 + 2SK544 AND 2SJ45 + 2SK163 WITH DIFFERENT LOAD RESISTANCES R_L

FET	R_L kΩ	$R_L + R_{FET,a}$ kΩ	$R_L + R_{FET,g}$ kΩ	Theoretical MF	Measured MF
2SJ44	4.7	4.85	28.55	5.9	5.3
	6.0	6.40	32.47	5.1	5.1
	10.0	29.34	75.74	2.6	2.7
2SK544	4.7	5.00	28.98	5.8	5.5
	6.0	6.62	30.94	4.7	5.2
	10.0	26.79	51.69	1.9	2.4
2SJ44+ 2SK544	6.0	6.81	46.15	6.8	7.5
2SJ45+ 2SK163	6.0	9.82	58.02	5.9	5.1

0.1 to 3 ppm are enhanced greatly by the p-FET amplification circuit. The magnification factors are shown in Figure 3c by testing at least 6 sensors. It illustrates that maximum apparent response and magnification factors are obtained using the 6.0 kΩ resistor when concentrations of xylene are lower than 0.5 ppm. The magnification factors are 3-5 depending on gas concentrations because varied gas concentrations would generate different gate voltages of the FET 2SJ44 and thus make it work on different resistances.

Quantitatively, the magnification factor (MF) is the change of the total resistance ($R_L + R_{FET}$), which can be calculated by the formula $(R_L + R_{FET,g})/(R_L + R_{FET,a})$ [42]. $(R_L + R_{FET})$ can be estimated by two methods: the first one is that it is plotted by V_{OUT}/I, where $V_{OUT} = -V_{DS} + V_{GS}$ from the p-type FET viewpoint in Figure 1. The V_{OUT} can be estimated by the $I_{DS} - V_{DS}$ curves of FET 2SJ44 at different V_{GS} as shown in Fig. S2a. In the meanwhile, in the series circuit of ohmic law $R = U/I$, $(R_L + R_{FET})$ can also be calculated by the equation $(R_L + R_{FET}) = 5/I - R_{S,a}$ as shown in Figure 3d (black line) with typical measured $R_{S,a} = 45$ kΩ of the sensor (more details about Figure 3d are shown in Supporting Information Figure S1). The intersection points of these two curves $(R_L + R_{FET}) = V_{OUT}/I = 5/I - R_{S,a}$ are the values of $(R_L + R_{FET,a})$. It is found that the value of $(R_L + R_{FET,a})$ is about 4.85 kΩ when R_L is 4.7 kΩ with FET 2SJ44 inferring the ON state of the FET with resistance of only 0.15 kΩ. On the other side, when the gas sensor is exposed to 0.5 ppm xylene, the value of $R_{S,0.5ppm}$ is 6.7 kΩ (response to 0.5 ppm is ~6.7 in Figure 3b, and $R_{S,0.5ppm} = 45$ kΩ/6.7). Similarly, the value of $(R_L + R_{FET,0.5ppm})$ can be calculated by the intersection points $(R_L + R_{FET}) = V_{OUT}/I = 5/I - R_{S,0.5ppm}$ in Figure 3d. The value of $(R_L + R_{FET,0.5ppm})$ is about 28.40 kΩ. Thus, the MF is calculated to be 28.40 kΩ/6.7 kΩ = 5.9. It should be noted that when R_L is 6.0 kΩ, there is no intersection points between the curve of $(R_L + R_{FET}) - I$ and the curve $(R_L + R_{FET}) = 5/I - R_{S,0.5ppm}$, which means that $(R_L + R_{FET,0.5ppm})$ has reached the saturation value 32.47 kΩ and the $R_L + R_{FET,a}$ value is about 6.40 kΩ as seen in Figure 3d. Thus the MF is 32.47 kΩ/6.4 kΩ = 5.1. Some maximum values of $(R_L + R_{FET,g})$ and initial values of $(R_L + R_{FET,a})$ are listed in Table 1. Then MF can be easily estimated by the resistance change, as shown in Table 1. It is noticed that

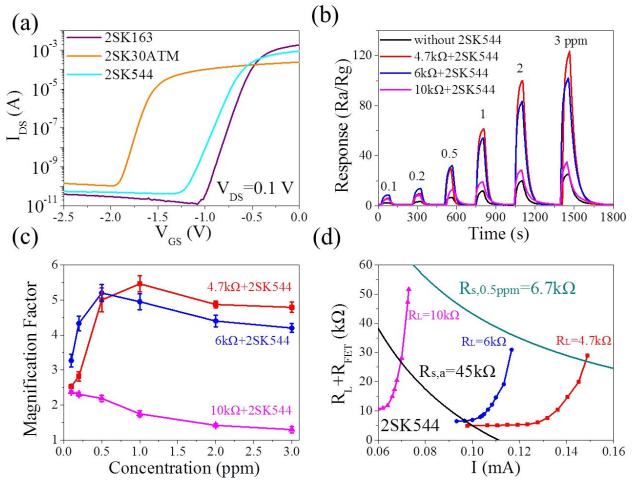

Fig. 4. Amplification effect of n-FET amplification circuits: (a) I_{DS}-V_{GS} curves of FETs 2SK544, 2SK163 and 2SK30ATM, (b) response of TGS2602 to xylene from 0.1 to 3 ppm in the electric circuit with and without FET 2SK544, (c) magnification factors of the amplification circuit with FET 2SK544, and (d) the curves of ($R_L + R_{FET}$) – I by connecting resistors of R_L = 4.7, 6.0 and 10.0 kΩ. The intersection points with 5/I – $R_{S,a}$ and 5/I – $R_{S,0.5ppm}$ curves are the ($R_L + R_{FET}$) value in air and in 0.5 ppm xylene.

these estimated theoretical MF are in good consistence with those observed. Figure 3d shows that the $R_L + R_{FET,a}$ value (about 6.40 kΩ) is similar to R_L = 6.0 kΩ without FET 2SJ44 (at ON state, R_{FET} is ∼ 0.4 kΩ). This means the FET has neglectable impact on the baseline in clean air, which is the main reason why this p-FET amplification circuit could not amplify the noise. Therefore, the p-FET amplification circuit can now work well for the MOX sensors from both mechanism and technological aspects, with the largest MF of ∼5.

B. n-FET amplification circuit

The n-FET amplification circuit has been studied in our previous work with similar MF of 5-6 in detection of toluene, acetone and ethanol [42]. In this paper, more n-FETs (2SK163 and 2SK30ATM) are explored in an aim to amplify the apparent response to xylene, with different R_L (4.7, 6.0 and 10.0 kΩ). Figure 4a shows the typical transfer curves of these n-FET devices, which can effectively amplify the apparent response to xylene as compared in Figure 4b. The largest MF is also calculated to be 5-6 as shown in Figure 4c, which is also in good accordance with those theoretically estimated in Figure 4d (more details shown in Figure S2). All these results show the similar amplification effect in detecting xylene using the n-FET 2SK544 compared to p-FET.

C. Synergetic p+n amplification circuit

From Figure 3b, c and Figure 4b, c, it should be noted that maximum response values and magnification factors are obtained using the 6.0 kΩ resistor when concentrations of xylene are lower than 0.5 ppm. Therefore, the value of R_L is chosen to be 6.0 kΩ in the p+n amplification circuit which combines p-type FET 2SJ44 and n-type 2SK544 as connected in Figure 1. As shown in Figure 5a and b, it is obvious that output voltages and apparent response value to xylene are enhanced greatly by the p+n amplification circuits.

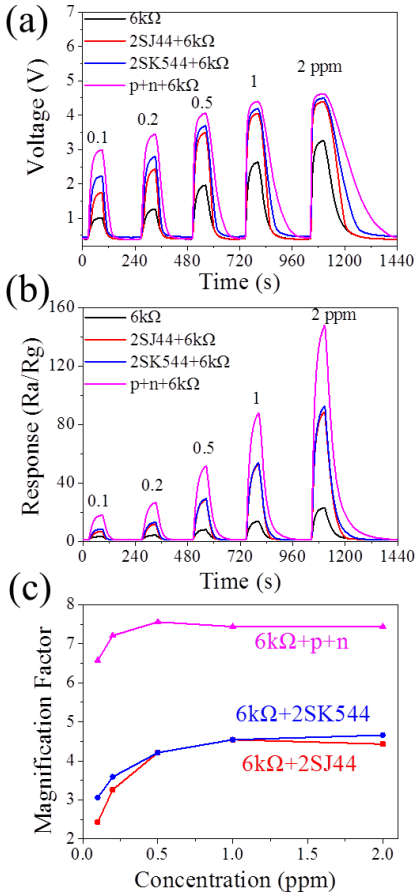

Fig. 5. Amplification effect of synergetic p+n amplification circuit. Comparison of (a) output voltage and (b) the calculated response among the circuits with FET 2SJ44, FET 2SK544, FETs 2SJ44+2SK544, and without FET by connecting resistor of R_L = 6.0 kΩ, and (c) magnification effect comparison among p-FET amplification, n-FET amplification, and synergetic p+n amplification circuits.

The MF curves are shown in Figure 5c by testing at least 6 sensors, where it is obvious that MFs of p+n amplification circuit (∼7.5) exceed greatly those of single p- and n-FET amplification circuits (∼5).

To explore more available p+n circuits, three couples of p- and n-FETs with similar threshold voltages and subthreshold swings are adopted to detect the xylene, with apparent responses and MFs shown in Figure 6. It is clearly shown that the couple of 2SJ44 + 2SK544 works more excellently than other two couples of FETs (2SJ45 + 2SK163 and 2SJ164 + 2SK30ATM), as details shown in Figures S3-6 in supporting information. It should be noted that the p- and n-FETs should be well chosen as to be integrated into an effective synergetic p+n amplification circuit. For example, 2SJ44+2SK544 couple has higher MF than those single ones, while 2SJ45+2SK544 couple has similar MF with single ones (Figure S7), meaning only one FET works in this couple. We further study how a p-type FET and an n-type FET could match successfully among various FETs. Figure 7 illustrates ($R_L + R_{FET}$) curves of two p-type FETs (2SJ44 and 2SJ45) and two n-type FETs (2SK544 and 2SK163). It is found that 2SJ45 and 2SK163 FETs match well because their (R_L+R_{FET}) curves nearly coincide with each other, and so do 2SJ44

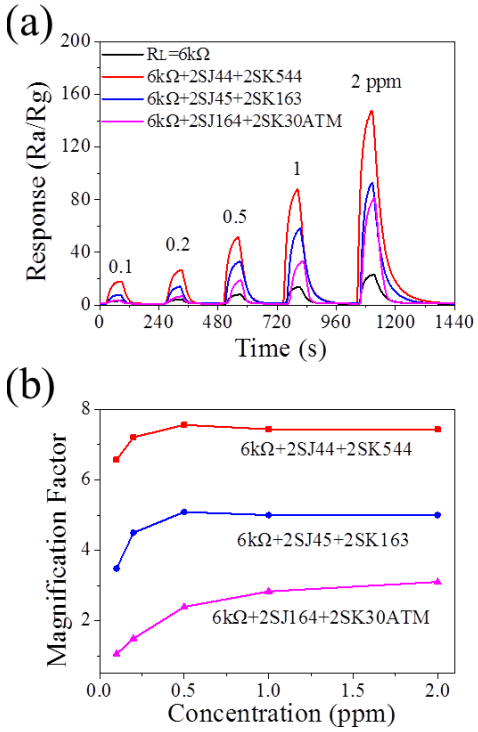

Fig. 6. Amplification effect of synergetic p+n amplification circuit. Comparison of (a) the calculated response and (b) magnification effect among three p+n amplification circuits with a couple of FETs (2SJ44+2SK544, 2SJ45+2SK163, and 2SJ164+2SK30ATM) by connecting resistor of $R_L = 6.0$ kΩ.

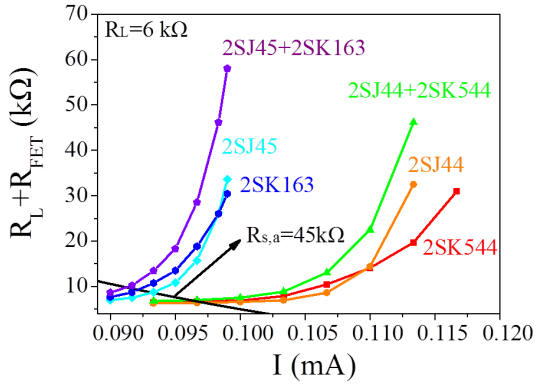

Fig. 7. Amplification mechanism of synergetic p+n amplification circuits.

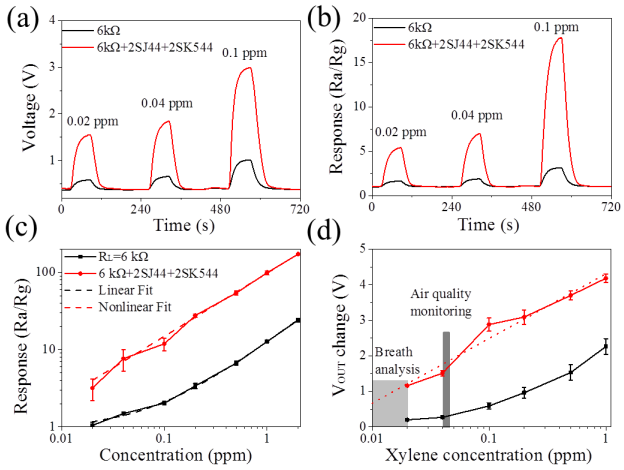

Fig. 8. Comparison of (a) output voltage and (b) response to 0.02 and 0.04 ppm xylene, (c) response and (d) voltage curves to xylene gas from 0.02 to 2 ppm between the traditional circuit and the synergetic p+n amplification one by connecting 6.0 kΩ resistor. Solid lines are experimental data and dash lines are fitted ones. Fitting formula in (c) are $S = 0.93 + 11.80 \times c$ (red solid line, $R^2 = 0.9995$) and $S = 97.99 \times c^{0.818}$ (dash solid line, $R^2 = 0.999$), respectively.

and 2SK544. This guarantees that the matched couple of FETs work synchronically to induce the optimum amplification effect of p+n circuit. Their MFs are listed in Table 1. It should be noted that both p-type 2SJ44 and 2SJ45 have similar transfer curves as shown in Figure 3a and thus are complementary to n-type 2SK544 in traditional CMOS. However, once 2SJ45 and 2SK544 FETs are integrated in p+n amplification circuits, it is expected that 2SJ45 FET will work and become saturated firstly at low current (<0.1 mA) while 2SK544 does not work at the moment seen in Figure 7 and Figure S7 (the two FETs are connected in series and thus should have the same current), which makes failure of the synergetic p+n amplification circuits. Nor can the other combinations of p+n FETs work synergistically to enhance the signal. In all, the amplification effect in p+n circuit is obtained if ($R_L + R_{FET}$) curves of p- and n-type FETs nearly coincide with each other.

The optimized p+n amplification circuit is then used to test the response to xylene with lower concentration such as 20 and 40 ppb as shown in Figure 8. A significant voltage response can be seen in the response curve in Figure 8a with the couple of FET 2SJ44+2SK544. Otherwise, the voltage change is neglectable to 20 and 40 ppb xylene in the conventional circuit. The apparent responses are calculated in Figure 8b, where it is clear that responses of 5.4, 7.0 and 17.8 are obtained to 20, 40 and 100 ppb xylene, much higher than those without FET. Figure 8c shows the fitting curves versus concentration, which derives the response of response to xy2.3 to 10 ppb xylene.

As the voltage signal is adopted in electronic circuits, we also plotted the voltage signal in Figure 8d. If we set a background error of 0.1 V (noise < 0.01 V as shown in Figure S8) in detecting the voltage, then 0.3 V voltage should be taken as the effective signal (S/N = 3). It is clear that the voltage signal is >0.5 V for the 10 ppb xylene, meaning the good resolution at this level. It should be noted that this detection limit is more than one order of magnitude lower than the human's olfactory threshold of 470 ppb [49]. China (GB/T 18883-2002) recommends a maximum permitted limit of 0.2 mg/m^3 (42 ppb) xylene in indoor air. Therefore, whether the xylene concentration is above the standard in indoor air can be easily assessed using the p+n amplification circuit with detection limit of ~10 ppb. And more importantly, all the electronics can be readily purchased from the market and be integrated easily onto a board.

To measure the cross sensitivity of the sensor, some typical gases are tested in this study including toluene (TGS2602 is designed for toluene in the manual as it is often used as the total organic volatile compounds equivalent concentration for air contaminants [50], [51]), benzene, acetone,

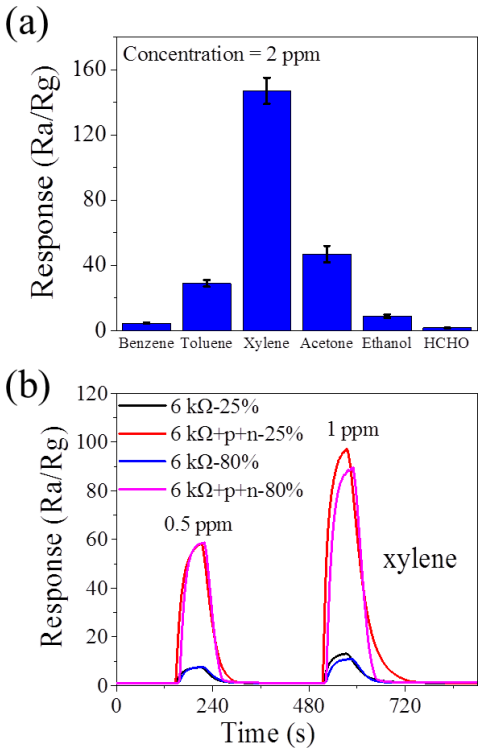

Fig. 9. (a) The response to 2 ppm six types of target gases (Benzene, toluene, xylene, acetone, ethanol and HCHO). (b) Comparison of response to 0.5 ppm and 1 ppm xylene in the circuits with FETs 2SJ44+2SK544, and without FET by connecting 6.0 kΩ resistor in different humid atmospheres (25% and 80%).

ethanol, formaldehyde and relative humidity (RH) as shown in Figure 9 and Figures S9-13 in supporting information. It is clear that the response to xylene is far higher than those to benzene, toluene, acetone, ethanol and formaldehyde as shown in Figure 9a. Though the response to toluene is up to 20% of that to xylene, the cross sensitivity is not so important as toluene is also one of biomarkers related to lung cancer [3], [47]. However, the cross sensitivity is neglectable to formaldehyde, which is one typical volatile organic compound (VOC) for breast cancer [3], [48]. The largest interference comes from acetone, which however induces only $<1/3$ of the response to xylene. Last but not least, in a high humid atmosphere of RH 80%, the gas sensing performance to xylene is similar to those in RH 25% as shown in Figure 9b. Therefore, the FET amplification circuits can make TGS2602 gas sensor very helpful for early stage real-time diagnosis of lung cancer.

In short, the p+n amplification circuit could make TGS2602 gas sensors show higher response to xylene than traditional ones. At the same time, the p+n amplification circuits can extend the detection limit of TGS2602 to ~10 ppb xylene. Data listed in Table 2 show comparison of some typical xylene sensors. It is noticeable that these commercial sensors working in p+n amplification circuits are already ones of the highest responses and most importantly, they can be readily used for trace concentration gas detection integrated in a large scale. It is also noted that the response time of 30-40 s is not influenced by FET amplification circuits as shown in Table S1.

TABLE II
COMPARISON OF THE TYPICAL XYLENE SENSORS

Sensor type	Conc. (ppm)	Response (Ra/Rg)	Reference
TGS2602	1	~11.8	
	1	~52 with 2SK544	This work
	1	~54 with 2SJ44	This work
	1	~88 with 2SJ44 and 2SK544	This work
	0.01	~2.3 with 2SJ44 and 2SK544	This work
α-MoO_3/α-Fe_2O_3 heterostructures	5	~5	[29]
Pd-loaded SnO_2 yolk–shell spheres	1	~9	[30]
Pd-loaded Co_3O_4 Hollow nanostructures	5	~361	[31]
Ni-doped TiO_2 bowllike particles	100	~5	[32]
Co-doped branched ZnO nanowires	5	~20	[33]
Cr-doped NiO hierarchical nanostructures	5	~12	[34]
Double-layered thin film	0.07	~2	[35]

However, recovery time is prolonged by several seconds, which may be due to the superposition of two hysteresis loops in I_{DS}-V_{GS} curves of FETs 2SJ44 and 2SK544 where the current circle varies from 0.1 mA to 0.12 mA as seen in Figure S14 in supporting information. In the meanwhile, the cost increase by this p+n FET circuit is only around 10% of the sensor. Therefore, this signal amplification circuit is promising for the fast and effective detection of xylene. Moreover, this synergetic p+n FET amplification circuits can also be adopted to detection of other gases with enhanced responses such as toluene, acetone and ethanol as shown in Figures S9-13 in the supporting information.

V. CONCLUSION

The ppb-level xylene detection for air quality monitoring and breath analysis using metal oxide semiconductor (MOX) gas sensors is successfully completed by our proposed synergetic p+n amplification circuits. The amplification mechanism is found to be the resistance change of the FET induced by the gate voltage. Besides, synergetic p+n amplification circuits can not only improve the sensor's response to different concentrations of xylene, but also decrease the detection limit of TGS2602 sensor to ~10 ppb xylene. Further study indicates that amplification effect of synergetic p+n circuits is ascribed to the fact that ($R_L + R_{FET}$) curves of p- and n-type FETs nearly coincide with each other, which guarantees that the matched couple of FETs work synchronically. In the meanwhile, the sensor shows also good selectivity over formaldehyde, one typical gas exhaled by breast cancers and relative humidity existing in breath. In a word, the signal amplification circuits above show the advantage in low concentration gas detection in environment and health. And these circuit designs are also promising in other kind of sensors to extend the detection limit to low concentrations.

REFERENCES

[1] A. Sarafraz-Yazdi, G. Rounaghi, I. Razavipanah, H. Vatani, and A. Amiri, "New polypyrrole–carbon nanotubes–silicon dioxide solid-phase microextraction fiber for the preconcentration and determination of benzene, toluene, ethylbenzene, and o-xylene using gas liquid chromatography," *J. Separat. Sci.*, vol. 37, no. 18, pp. 2605–2612, Sep. 2014.

[2] B. Wang *et al.*, "A highly sensitive diketopyrrolopyrrole-based ambipolar transistor for selective detection and discrimination of xylene isomers," *Adv. Mater.*, vol. 28, no. 21, pp. 4012–4018, Jun. 2016.

[3] G. Peng *et al.*, "Diagnosing lung cancer in exhaled breath using gold nanoparticles," *Nature Nanotechnol.*, vol. 4, no. 10, pp. 669–673, Oct. 2009.

[4] S. Zhao *et al.*, "A colorimetric detector for lung cancer related volatile organic compounds based on cross-response mechanism," *Sens. Actuators B, Chem.*, vol. 256, pp. 543–552, Mar. 2018.

[5] T. Oguma *et al.*, "Clinical contributions of exhaled volatile organic compounds in the diagnosis of lung cancer," *PLoS ONE*, vol. 12, no. 4, p. e0174802, 2017.

[6] W. Ma, P. Gao, J. Fan, Y. Hashi, and Z. Chen, "Determination of breath gas composition of lung cancer patients using gas chromatography/mass spectrometry with monolithic material sorptive extraction," *Biomed. Chromatogr.*, vol. 29, no. 6, pp. 961–965, Jun. 2015.

[7] M. Girschikofsky, M. Rosenberger, S. Belle, M. Brutschy, S. R. Waldvogel, and R. Hellmann, "Optical planar Bragg grating sensor for real-time detection of benzene, toluene and xylene in solvent vapour," *Sens. Actuators B, Chem.*, vols. 171–172, pp. 338–342, Aug./Sep. 2012.

[8] E. C. Nallon, V. P. Schnee, C. J. Bright, M. P. Polcha, and Q. Li, "Discrimination enhancement with transient feature analysis of a graphene chemical sensor," *Anal. Chem.*, vol. 88, no. 2, pp. 1401–1406, Dec. 2016.

[9] A. D. Rushi, K. P. Datta, P. S. Ghosh, A. Mulchandani, and M. D. Shirsat, "Selective discrimination among benzene, toluene, and xylene: Probing metalloporphyrin-functionalized single-walled carbon nanotube-based field effect transistors," *J. Phys. Chem. C*, vol. 118, no. 41, pp. 24034–24041, Oct. 2014.

[10] T. Xu, P. Xu, D. Zheng, H. Yu, and X. Li, "Metal-organic frameworks for resonant-gravimetric detection of trace-level xylene molecules," *Anal. Chem.*, vol. 88, no. 24, pp. 12234–12240, Nov. 2016.

[11] J. J. Langenfeld, S. B. Hawthorne, and D. J. Miller, "Quantitative analysis of fuel-related hydrocarbons in surface water and wastewater samples by solid-phase microextraction," *Anal. Chem.*, vol. 68, no. 1, pp. 144–155, Jan. 1996.

[12] D. W. Potter and J. Pawliszyn, "Detection of substituted benzenes in water at the pg/ml level using solid-phase microextraction and gas chromatography—Ion trap mass spectrometry," *J. Chromatogr.*, vol. 625, no. 2, pp. 247–255, Nov. 1992.

[13] M. Schweigkofler and R. Niessner, "Determination of siloxanes and VOC in landfill gas and sewage gas by canister sampling and GC-MS/AES analysis," *Environ. Sci. Technol.*, vol. 33, no. 20, pp. 3680–3685, Oct. 1999.

[14] P. Karlitschek, F. Lewitzka, U. Bunting, M. Niederkrüger, and G. Marowsky, "Detection of aromatic pollutants in the environment by using UV-laser-induced fluorescence," *Appl. Phys. B, Lasers Opt.*, vol. 67, no. 4, pp. 497–504, Oct. 1998.

[15] N. Yamazoe, "Toward innovations of gas sensor technology," *Sens. Actuators B, Chem.*, vol. 108, nos. 1–2, pp. 2–14, 2005.

[16] M. E. Franke, T. J. Koplin, and U. Simon, "Metal and metal oxide nanoparticles in chemiresistors: Does the nanoscale matter?" *Small*, vol. 2, no. 1, pp. 36–50, Jan. 2006.

[17] H.-R. Kim, A. Haensch, I.-D. Kim, N. Barsan, U. Weimar, and J.-H. Lee, "The role of NiO doping in reducing the impact of humidity on the performance of SnO_2-based gas sensors: Synthesis strategies, and phenomenological and spectroscopic studies," *Adv. Funct. Mater.*, vol. 21, no. 23, pp. 4456–4463, Dec. 2011.

[18] A. Kolmakov, Y. X. Zhang, G. S. Cheng, and M. Moskovits, "Detection of CO and O_2 using tin oxide nanowire sensors," *Adv. Mater.*, vol. 15, no. 12, pp. 997–1000, Jun. 2003.

[19] J.-H. Lee, "Gas sensors using hierarchical and hollow oxide nanostructures: Overview," *Sens. Actuators B, Chem.*, vol. 140, no. 1, pp. 319–336, 2009.

[20] N. Yamazoe, "New approaches for improving semiconductor gas sensors," *Sens. Actuators B, Chem.*, vol. 5, nos. 1–4, pp. 7–19, 1991.

[21] J.-W. Yoon, S. H. Choi, J.-S. Kim, H. W. Jang, Y. C. Kang, and J.-H. Lee, "Trimodally porous SnO_2 nanospheres with three-dimensional interconnectivity and size tunability: A one-pot synthetic route and potential application as an extremely sensitive ethanol detector," *NPG Asia Mater.*, vol. 8, p. e244, Mar. 2016.

[22] Y. Lü *et al.*, "MOF-templated synthesis of porous Co_3O_4 concave nanocubes with high specific surface area and their gas sensing properties," *ACS Appl. Mater. Interfaces*, vol. 6, no. 6, pp. 4186–4195, Mar. 2014.

[23] J. Guo, J. Zhang, M. Zhu, D. Ju, H. Xu, and B. Cao, "High-performance gas sensor based on ZnO nanowires functionalized by Au nanoparticles," *Sens. Actuators B, Chem.*, vol. 199, pp. 339–345, Apr. 2014.

[24] Y.-X. Li *et al.*, "Hierarchical morphology-dependent gas-sensing performances of three-dimensional SnO_2 nanostructures," *ACS Sensors*, vol. 2, no. 1, pp. 102–110, Jan. 2017.

[25] D. Chen, J. Xu, Z. Xie, and G. Z. Shen, "Nanowires assembled SnO_2 nanopolyhedrons with enhanced gas sensing properties," *ACS Appl. Mater. Interfaces*, vol. 3, no. 6, pp. 2112–2117, May 2011.

[26] J. Rao, A. Yu, C. Shao, and X. Zhou, "Construction of hollow and mesoporous ZnO microsphere: A facile synthesis and sensing property," *Acs Appl. Mater. Interfaces*, vol. 4, no. 10, pp. 5346–5352, Oct. 2012.

[27] D. Degler *et al.*, "Gold-loaded tin dioxide gas sensing materials: Mechanistic insights and the role of gold dispersion," *ACS Sensors*, vol. 1, no. 11, pp. 1322–1329, Nov. 2016.

[28] M. Hjiri, L. El Mir, S. G. Leonardi, A. Pistone, L. Mavilia, and G. Neri, "Al-doped ZnO for highly sensitive CO gas sensors," *Sens. Actuators B, Chem.*, vol. 196, pp. 413–420, Jun. 2014.

[29] D. S. Jiang *et al.*, "Xylene gas sensor based on α-MoO_3/α-$Fe_2 3O_3$ heterostructure with high response and low operating temperature," *RSC Adv.*, vol. 5, no. 49, pp. 39442–39448, 2015.

[30] Y. J. Hong, J.-W. Yoon, J.-H. Lee, and Y. C. Kang, "One-pot synthesis of pd-loaded SnO_2 yolk–shell nanostructures for ultraselective methyl benzene sensors," *Chem., Eur. J.*, vol. 20, no. 10, pp. 2737–2741, Mar. 2014.

[31] S.-J. Hwang, K.-I. Choi, J.-W. Yoon, Y. C. Kang, and J.-H. Lee, "Pure and palladium-loaded Co_3O_4 hollow hierarchical nanostructures with giant and ultraselective chemiresistivity to xylene and toluene," *Chem., Eur. J.*, vol. 21, no. 15, pp. 5872–5878, Apr. 2015.

[32] L. Zhu *et al.*, "Xylene gas sensor based on Ni doped TiO_2 bowl-like submicron particles with enhanced sensing performance," *RSC Adv.*, vol. 5, no. 36, pp. 28105–28110, 2015.

[33] H.-S. Woo, C.-H. Kwak, J.-H. Chung, and J.-H. Lee, "Co-doped branched ZnO nanowires for ultraselective and sensitive detection of xylene," *ACS Appl. Mater. Interfaces*, vol. 6, no. 24, pp. 22553–22560, Dec. 2014.

[34] H.-J. Kim, J.-W. Yoon, K.-I. Choi, H. W. Jang, A. Umar, and J.-H. Lee, "Ultraselective and sensitive detection of xylene and toluene for monitoring indoor air pollution using Cr-doped NiO hierarchical nanostructures," *Nanoscale*, vol. 5, no. 15, pp. 7066–7073, 2013.

[35] T. Akiyama, Y. Ishikawa, and K. Hara, "Xylene sensor using double-layered thin film and Ni-deposited porous alumina," *Sens. Actuators B, Chem.*, vol. 181, pp. 348–352, May 2013.

[36] M. Leidinger, M. Rieger, T. Sauerwald, C. Alépée, and A. Schütze, "Integrated pre-concentrator gas sensor microsystem for ppb level benzene detection," *Sens. Actuators B, Chem.*, vol. 236, pp. 988–996, Nov. 2016.

[37] J. W. Gardner, P. K. Guha, F. Udrea, and J. A. Covington, "CMOS interfacing for integrated gas sensors: A review," *IEEE Sensors J.*, vol. 10, no. 12, pp. 1833–1848, Dec. 2010.

[38] X. F. Liang and L. H. Liu, "Design on the amplifier circuit of metal-oxide semiconductor gas-sensitive sensor," *Appl. Mech. Mater.*, vols. 220–223, pp. 1939–1942, Nov. 2012.

[39] C. Falconi *et al.*, "Electronic interfaces," *Sens. Actuators B, Chem.*, vol. 121, no. 1, pp. 295–329, Jan. 2007.

[40] A. Lombardi *et al.*, "A CMOS integrated interface circuit for metal-oxide gas sensors," *Sens. Actuators B, Chem.*, vol. 142, no. 1, pp. 82–89, 2009.

[41] Y.-D. Wang, X.-H. Wu, and Z.-L. Zhou, "Novel high sensitivity and selectivity semiconductor gas sensor based on the p+n combined structure," *Solid-State Electron.*, vol. 44, no. 9, pp. 1603–1607, 2000.

[42] X. Zhou *et al.*, "Amplifying the signal of metal oxide gas sensors for low concentration gas detection," *IEEE Sensors J.*, vol. 17, no. 9, pp. 2841–2847, May 2017.

[43] R. Q. Xing *et al.*, "Preparation and gas sensing properties of In_2O_3/Au nanorods for detection of volatile organic compounds in exhaled breath," *Sci. Rep.*, vol. 5, Jun. 2015, Aty. no. 10717.

[44] Y. Guan *et al.*, "Hydrothermal preparation and gas sensing properties of Zn-doped SnO2 hierarchical architectures," *Sens. Actuators B, Chem.*, vol. 191, pp. 45–52, Feb. 2014.
[45] S. L. Bai *et al.*, "Preparation of reduced graphene oxide/Co_3O_4 composites and sensing performance to toluene at low temperature," *RSC Adv.*, vol. 6, no. 65, pp. 60109–60116, 2016.
[46] N. Qin, X. H. Wang, Q. Xiang, and J. Q. Xu, "A biomimetic nest-like ZnO: Controllable synthesis and enhanced ethanol response," *Sens. Actuators B, Chem.*, vol. 191, pp. 770–778, Feb. 2014.
[47] N.-H. Kim, S.-J. Choi, D.-J. Yang, J. Bae, J. Park, and I.-D. Kim, "Highly sensitive and selective hydrogen sulfide and toluene sensors using Pd functionalized WO_3 nanofibers for potential diagnosis of halitosis and lung cancer," *Sens. Actuators B, Chem.*, vol. 193, pp. 574–581, Mar. 2014.
[48] S. E. Ebeler, A. J. Clifford, and T. Shibamoto, "Quantitative analysis by gas chromatography of volatile carbonyl compounds in expired air from mice and human," *J. Chromatogr. B, Biomed. Sci. Appl.*, vol. 702, pp. 211–215, Nov. 1997.
[49] G. Leonardos, D. Kendall, and N. Barnard, "Odor threshold determination of 53 odorant chemicals," *J. Air Pollution Control Assoc.*, vol. 19, no. 2, pp. 91–95, 1969.
[50] C. Badji, J. Beigbeder, H. Garay, A. Bergeret, J.-C. Bénézet, and V. Desauziers, "Under glass weathering of hemp fibers reinforced polypropylene biocomposites: Impact of volatile organic compounds emissions on indoor air quality," *Polymer Degradation Stability*, vol. 149, pp. 85–95, Mar. 2018.
[51] M. Chang *et al.*, "Prenatal TVOCs exposure negatively influences postnatal neurobehavioral development," *Sci. Total Environ.*, vol. 618, pp. 977–981, Mar. 2018.

Xinyuan Zhou received the B.S. degree in materials chemistry from the Taiyuan University of Technology in 2010. He is currently pursuing the Ph.D. degree in materials engineering with the Institute of Process Engineering, CAS.

Ying Wang received the bachelor's degree in optics from Beijing Jiaotong University in 2010 and the Ph.D. degree in physical electronics from the College of Electronics, Peking University, in 2015. She is currently an Assistant Professor with the Institute of Process Engineering, CAS.

Zhou Wang received the bachelor's degree in chemical engineering and technology from the Wuhan Institute of Technology. He is currently pursuing the M.S. degree with the Beijing University of Chemical Technology.

Liping Yang received the Ph.D. degree in chemical engineering from the Institute of Chemistry, CAS, in 2016. She holds a post-doctoral position at the Institute of Process Engineering, CAS, carrying out gas sensing material research.

Xiaofeng Wu received the Ph.D. degree from the Institute of Process Engineering, Chinese Academy of Sciences, in 2007. After Post-Doctoral Research at Chonbuk National University, South Korea, he joined the Institute of Process Engineering in 2009, where he is currently a Professor. His research interests are the preparation of nanostructural inorganic materials (metal–oxide–semiconductor core–shell hollow particles and so on) and their application in sensors, photocatalysis, thermal insulator, and energy storage.

Ning Han received the Ph.D. degree in chemical engineering from the Institute of Process Engineering, CAS, in 2010. He was a Post-Doctoral Fellow with the Department of Physics and Materials Science, City University of Hong Kong, from 2010 to 2014. He has been a Professor with IPE CAS via One Hundred Talents Plan since 2014. He is works on investigations of preparation, structure, and property of semiconductors, and has developed highly sensitive and selective gas sensing materials. He has authored over 80 articles.

Yunfa Chen received the Ph.D. degree in material science from the Université Louis Pasteur Strasbourg, France, in 1993. He is currently a Professor with the Graduate University of Chinese Academy of Sciences, and a Research Professor and the Vice Director of the Institute of Process Engineering, Chinese Academy of Sciences. His current research interests are the preparation and assembly of nanoparticles, functional materials, organic–inorganic composite materials and layered materials, and industrial application of nanomaterials.